MIT Libraries | DSpace@MIT

MIT Open Access Articles

# *Storage of charge carriers on emitter molecules in organic light-emitting diodes*

The MIT Faculty has made this article openly available. ***Please share*** how this access benefits you. Your story matters.

**Citation:** Weichsel, Caroline et al. "Storage of Charge Carriers on Emitter Molecules in Organic Light-emitting Diodes." Physical Review B 86.7 (2012). ©2012 American Physical Society

**As Published:** http://dx.doi.org/10.1103/PhysRevB.86.075204

**Publisher:** American Physical Society

**Persistent URL:** http://hdl.handle.net/1721.1/74266

**Version:** Final published version: final published article, as it appeared in a journal, conference proceedings, or other formally published context

**Terms of Use:** Article is made available in accordance with the publisher's policy and may be subject to US copyright law. Please refer to the publisher's site for terms of use.

Massachusetts Institute of Technology

# Storage of charge carriers on emitter molecules in organic light-emitting diodes

Caroline Weichsel,* Lorenzo Burtone, Sebastian Reineke,† Susanne I. Hintschich, Malte C. Gather, Karl Leo, and Björn Lüssem

*Institut für Angewandte Photophysik, Technische Universität Dresden, George-Bähr-Str. 1, 01062 Dresden, Germany*

(Received 3 April 2012; revised manuscript received 20 June 2012; published 13 August 2012)

Organic light-emitting diodes (OLEDs) using the red phosphorescent emitter iridium(III)bis(2-methyldibenzo[f,h]quinoxaline) (acetylacetonate) [Ir(MDQ)$_2$(acac)] are studied by time-resolved electroluminescence measurements. A transient overshoot after voltage turn-off is found, which is attributed to electron accumulation on Ir(MDQ)$_2$(acac) molecules. The mechanism is verified via impedance spectroscopy and by application of positive and negative off-voltages. We calculate the density of accumulated electrons and find that it scales linearly with the doping concentration of the emitter. Using thin quenching layers, we locate the position of the emission zone during normal OLED operation and after voltage turn-off. In addition, the transient overshoot is also observed in three-color white-emitting OLEDs. By time- and spectrally resolved measurements using a streak camera, we directly attribute the overshoot to electron accumulation on Ir(MDQ)$_2$(acac). We propose that similar processes are present in many state-of-the-art OLEDs and believe that the quantification of charge carrier storage will help to improve the efficiency of OLEDs.

DOI: 10.1103/PhysRevB.86.075204 PACS number(s): 81.05.Fb, 72.20.Jv, 73.50.Gr, 85.60.Jb

## I. INTRODUCTION

It is well known that excessive charge carrier densities in the emission layer (EML) of organic light-emitting diodes (OLEDs) can lead to significant triplet-polaron annihilation[1] and field-induced quenching.[2] However, until now, the possibility of charge accumulation in the EML has been mostly neglected, although this might have an equally important effect on device efficiency. Therefore, a technique to reliably determine and quantify charge carrier accumulation and storage inside the EML is most desirable.

A powerful tool for investigating charge carrier transport as well as exciton creation, transport, and annihilation is the time-resolved measurement of electroluminescence (EL) following a bias pulse. For instance, charge carrier mobilities may be determined from the onset of luminescence.[3,4] In addition, the measurement of postpulse transient luminescence provides information on exciton lifetimes and transfer processes.[5–7]

In this paper, we show that transient EL can also be used to study charge accumulation. We discuss the origin of the transient EL overshoot after voltage turn-off in a complex OLED structure containing doped transport layers. In fluorescent OLEDs, such transient overshoots are widely observed and investigated.[8–16] They are caused by a number of processes including delayed fluorescence created via triplet-triplet annihilation,[13–15] recombination of trapped charge carriers,[13] electric field-induced quenching,[16] or a change in the ratio of drift and diffusion currents during and after application of an electric field, which leads to enhanced recombination after turn-off.[8–10]

In phosphorescent OLEDs, a transient overshoot is typically attributed to a delayed recombination of trapped charge carriers.[16–19] Lin *et al*. observed a transient overshoot in a phosphorescent trilayer OLED and attributed this to interfacial trapping and detrapping on both sides of the electron-blocking layer (EBL).[19] Liu *et al*. report on a transient overshoot in phosphorescent systems with short emitter lifetimes, which they attribute to charge trapping on the emitter, however, without any further investigations of this system.[16] Reineke *et al*. observed delayed recombination in an aged *pin*-OLED stack and attribute their findings to electron accumulation on the phosphorescent emitter and poor hole injection caused by degradation.[17]

In this work, we show that charge carrier storage on emitter molecules also occurs in efficient, nondegraded phosphorescent state-of-the-art OLEDs. We investigate a red-emitting OLED stack by applying positive and negative turn-off voltages as well as a stepwise voltage pulse. Additionally, we measure the profile of the recombination zone and the impedance of the device and we vary the hole-blocking layer (HBL) and the doping concentration of the emitter. Based on the results from these various experiments, we are able to show that electrons accumulate on the red emitter at the interface to the EBL and are stored there. This storage effect also takes place in white phosphorescent OLEDs as shown by time- and spectrally resolved streak camera measurements. Further, we quantify this effect by calculating the density of the accumulated electrons. By combining the results from these different experiments, we gain a deeper understanding of the electronic processes taking place in the EML of phosphorescent OLEDs. We argue that charge carrier storage on emitter molecules can take place in many OLED structures and propose methods to identify and quantify this process.

## II. EXPERIMENTAL

All samples are prepared on precleaned glass substrates covered with 90 nm prepatterned indium tin oxide (ITO) stripes. All organic layers and the aluminum cathode are deposited by thermal evaporation in a UHV chamber (Kurt J. Lesker) with a base pressure of $10^{-8}$ mbar. The samples with a size of 6.49 mm$^2$ are encapsulated under nitrogen atmosphere with glass lids directly after preparation.

The used materials are purchased from various suppliers as stated below and further purified by high-vacuum gradient sublimation. The hole transport layer (HTL) consists of N,N,N′,N′-tetrakis-(4-methoxyphenyl)-benzidine

 ©2012 American Physical Society

[MeO-TPD, Sensient] doped with 4 wt.% 2,2′-(perfluoronaphthalene-2,6-diylidene)dimalononitrile [F6TCNNQ, Novaled AG]. As EBL 1,1-bis[(di-4-tolylamino)phenyl] cyclohexane [TAPC, Sensient] is used. The EML consists of TAPC-doped iridium(III)bis(2-methyldibenzo[f,h] quinoxaline)(acetylacetonate) [$Ir(MDQ)_2(acac)$, American Dye Source, Inc.], followed by a 2-(diphenylphosphoryl) spirofluorene [SPPO1, Lumtec] HBL. The electron transport layer (ETL) consists of Cs-doped 4,7-diphenyl-1,10-phenanthroline [BPhen, abcr GmbH & Co. KG]. The highest occupied molecular orbital (HOMO) and lowest unoccupied molecular orbital (LUMO) of TAPC,[20] SPPO1,[21] and $Ir(MDQ)_2(acac)$[22] are taken from the literature.

Voltage $V$, current density $j$, luminance $L$, and forward directed spectral radiant intensity $I_e(\lambda)$ are measured in an automated measurement setup containing a Keithley SM2400 source-measure unit, a calibrated silicon photodiode, and a calibrated CAS140CT spectrometer from Instrument Systems GmbH. The external quantum efficiency is calculated assuming a Lambertian emission profile.

50 $\mu$s voltage pulses are applied to the sample by an 8114-A pulse generator (Hewlett Packard) resulting in a typical current of 1 mA. We measure the resulting electroluminescence with a PDA10A-EC Si-photodiode (Thorlabs). All signals are detected by an infinium oscilloscope 54815A (Hewlett Packard). Typical pulse measurements are depicted in Fig. 1. The voltage applied to the sample is measured over a 1 MΩ resistance parallel to the OLED.[23] To obtain the current flow we record the voltage drop over a 50 Ω resistance connected in series with the OLED.

Time and spectrally resolved measurements are conducted using a C5680 streak camera with an M5677 sweep unit (Hamamatsu).

The impedance is measured with an Autolab PGSTAT302N applying a small sinusoidal signal (20 mV rms) superimposed on a constant bias voltage. The response in current is measured and the impedance is calculated from the ratio between voltage and current signals. By varying the bias voltage, it is possible to acquire a capacitance-voltage plot, whereas varying the frequency of the small signal gives a capacitance spectrum.

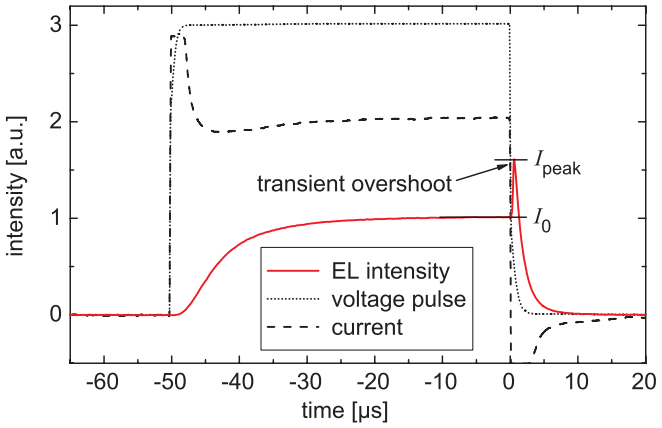


FIG. 1. (Color online) Pulse shapes of the collected pulses: EL signal measured by the photodiode (solid line), voltage pulse, as applied to the OLED (dotted line), and voltage drop over 50 Ω resistance to measure the current through the OLED (dashed line). The EL signal clearly shows a transient overshoot after voltage turn-off.

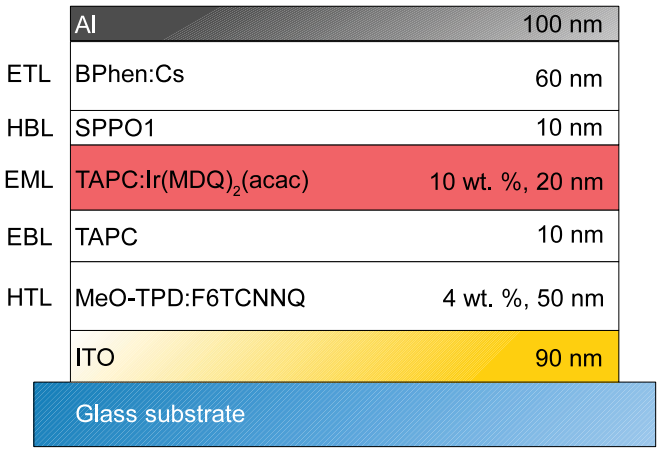


FIG. 2. (Color online) Schematic layer stack of the investigated OLED.

## III. RED-EMITTING OLEDs

The investigated OLED stack is based on a *pin*-structure[24,25] containing intrinsic blocking layers to confine the recombination of charge carriers to the emission layer (cf. Fig. 2). The 20 nm thick EML consists of 10 wt.% $Ir(MDQ)_2(acac)$-doped TAPC. As shown in Fig. 8 (solid lines), current sets in at approximately 2.6 V. 1000 cd/m$^2$ are reached at 4.5 V with an external quantum efficiency of 8.2%. We ascribe the lower efficiency compared to other structures using $Ir(MDQ)_2(acac)$[22] to charge carrier imbalance, caused by a large difference in hole mobility of TAPC[26] and electron mobility of SPPO1.[27] This imbalance is also visible in the initial increase of the efficiency at low currents.[28]

The time-resolved EL of this sample shows a transient overshoot after the voltage applied to the sample is turned off (cf. Fig. 1). In the following, we describe experiments to study the mechanism leading to this overshoot.

### A. Influence of the off-voltage

First, we investigate whether the overshoot in EL is caused by an electrical effect such as charge carrier accumulation or by a different mechanism. This is done by applying an off-voltage during the part of the pulse cycle when the main driving voltage is turned off. The off-voltage is smaller than the voltage applied during the first pulse and can be either positive or negative. Figure 3(a) shows the transient EL signal. The overshoot occurs earlier when applying negative voltages and later for positive voltages. Additionally, the peak height decreases for positive off-voltages.

The dependence of the signal on the off-voltage and the resulting electric field shows that the transient overshoot is indeed an electrical effect. Furthermore, we can exclude field-induced quenching during the on-state[16] as a possible reason because in this case changing the off-voltage would only lead to a variation in the peak height but not to a peak shift. Therefore, we conclude that electrons and holes accumulate at different interfaces inside the OLED. After turning the electric field off, the charge carriers are able to drift and diffuse

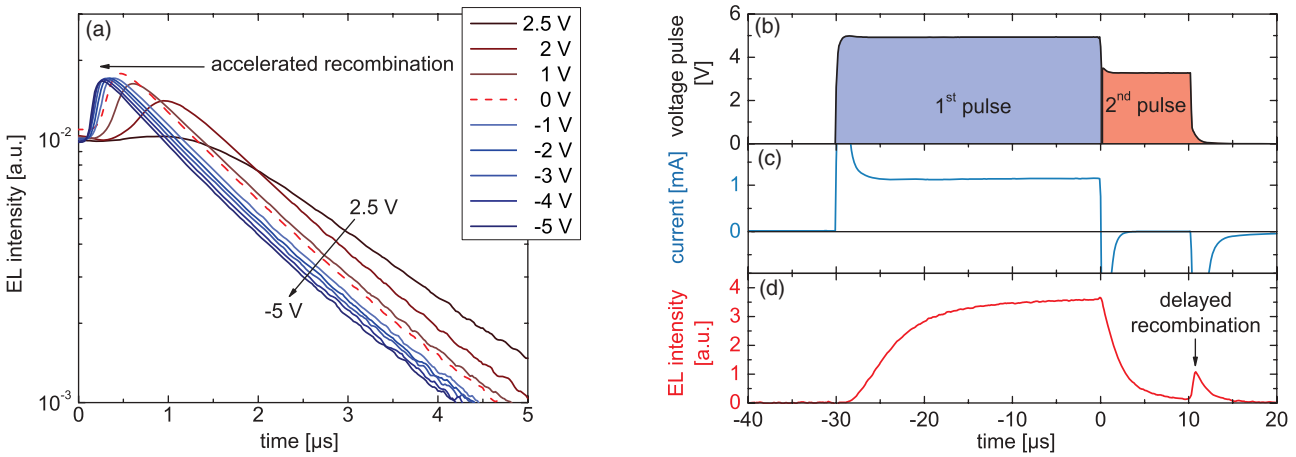


FIG. 3. (Color online) (a) Transient EL signal after main voltage pulse is turned off. Different voltages are applied in the off-state (from 2.5 V to −5 V). With negative voltages the recombination can be accelerated while a positive off-voltage leads to decelerated recombination. (b) Application of two voltage pulses to the OLED. The first pulse regularly drives the OLED while the second pulse prevents the accumulated charge carriers from recombining. (c) Current flow through the OLED. No current is measured during the second pulse. (d) EL intensity of the OLED. After turn-off of the first pulse no transient overshoot is visible. The delayed recombination only sets in when the second pulse is turned off.

freely and can then recombine causing a transient overshoot. As the appearance of the transient peak is accelerated when applying negative off-voltages and delayed when applying positive off-voltages, we deduce that electrons are located near the anode whereas holes accumulate near the cathode.

The time until the transient overshoot reaches its maximum $I_{peak}$ is mainly determined by the RC-time of the OLED (see Fig. 1 in Supplemental Material[29]).

The data shown in Fig. 3(a) indicate that the transient overshoot can be avoided by applying a positive off-voltage. This is reasonable since the positive electric field leads to a further storage of the charge carriers in their accumulation reservoir. Thus, we assume that the application of a sufficiently high temporary off-voltage should delay the transient overshoot until the off-voltage is turned off. To check this, we apply a 10 $\mu$s long off-voltage of 3.2 V by a DG535 (Stanford Research Systems, Inc.) directly after turning off the regular pulse. Figures 3(b)–3(d) show the applied voltage pulses, the measured current through the OLED, and the EL signal. The first pulse of 4.9 V drives the OLED regularly, leading to a current of 1 mA (current density: 15.4 mA/cm$^2$) through the OLED and to steady-state light emission. No overshoot is observed at the end of the first, regular pulse. Instead, the transient overshoot of the EL signal is shifted by 10 $\mu$s and appears after the end of the second pulse. A positive current flow is not detected during this pulse so that charge carrier injection can be excluded [cf. Fig. 3(c)]. The additional electric field thus prevents the accumulated charge carriers from recombining. Only after the end of the second pulse can the accumulated charge carriers recombine, leading to a transient overshoot. This effect is observed for pulse lengths of the second pulse up to 300 $\mu$s, indicating that charge carriers are not only accumulated, but also stored inside their reservoir.

### B. Emission zone profile

In the next step the location of the accumulated charge carriers inside the device is investigated. Regarding the HOMO and LUMO, electron- and hole-blocking materials provide sufficient energy barriers to block the electrons and holes, respectively (cf. Fig. 6). Therefore, we assume that electrons/holes cannot pass the EBL/HBL. As shown in Sec. III A, the accumulated electrons are positioned closer to the anode than the holes. We therefore assume that charge carrier storage takes place inside the EML, but outside the regular recombination zone. To confirm this assumption and to determine the precise location of the accumulated charges, we measured the profile of the emission zone during normal operation and after voltage turn-off. This was done by preparing samples containing a 0.5 nm thick quenching layer of fluorescent 3-(4-(diphenylamino)phenyl)-1-phenylprop-2-en-1-one [DPPO, CHESS GmbH], located at different positions within the EML. DPPO has a singlet energy level of 2.3 eV.[30] Assuming a singlet-triplet splitting of 0.3−0.4 eV[31] for the $n-\pi^*$ transition,[32] the triplet energy is expected to be below that of Ir(MDQ)$_2$(acac). Therefore, triplet excitons located on Ir(MDQ)$_2$(acac) near the DPPO layer are quenched nonradiatively and thus do not contribute to light emission. This so-called quenching method[1] requires that the electric behavior is not influenced so that only excitons transferred from the Ir(MDQ)$_2$(acac) molecules are quenched and no direct excitation of DPPO occurs.

The quenching layer of only 0.5 nm thickness does not form a closed layer and, therefore, does not change the electric properties, as confirmed by the unaffected current-voltage curves (see Supplemental Material,[29] Fig. 2). The triplet energy transfer from Ir(MDQ)$_2$(acac) to DPPO is a Dexter-type transfer, occurring only within a short distance of up to 2 nm.[7,33] This guarantees a high spatial resolution of the quenching method.

The quenching layer is inserted at different positions $x$ within the EML: $x = 0$ nm denotes the quenching layer at the EBL interface and $x = 20$ nm at the HBL interface. Emission spectrum and time-resolved EL intensity of all samples are measured.

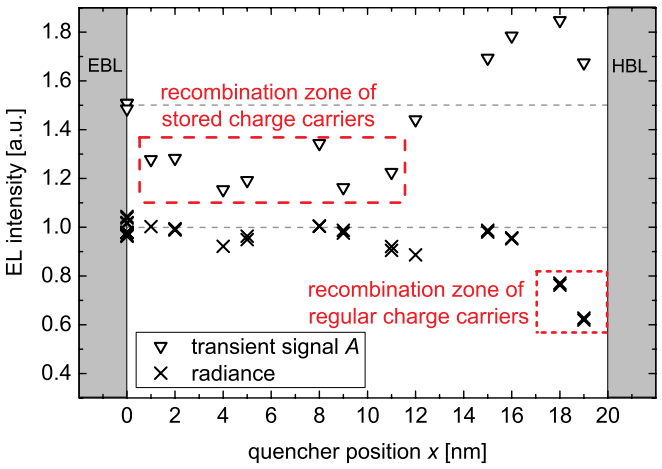


FIG. 4. (Color online) Emission radiance (crosses) and transient signal $A$ (triangles) of samples containing a thin quencher at different positions inside the EML at an applied current of 1 mA. Data points at $x = 0$ nm correspond to samples without quencher. Low intensity corresponds to a strong quenching of luminescence due to high local exciton densities. During normal OLED operation, high exciton densities are found at the HBL side, while the recombination of stored charge carriers occurs close to the EBL.

Figure 4 shows the emission radiance (crosses) for different positions of the quencher, normalized to the intensity of samples without the quencher (plotted at $x = 0$ nm). Several nominally identical samples were compared, showing a good reliability of the experiment. The lowest emission occurs for samples in which the quencher is located near the HBL. Low emission indicates high quenching rates and therefore high local exciton density. Therefore, we can reliably conclude that the recombination zone is located at the HBL side of the EML. This is reasonable since TAPC primarily conducts holes[26] and the large LUMO energy barrier between SPPO1 and TAPC limits electron injection.

To determine the position of the recombination zone after voltage turn-off and thus the location of accumulated charges, we measured the transients of all samples. We assume that the amount of accumulated electrons and holes inside the EML as well as the amount of created excitons is independent of the position of the quenching layer. Instead, the quenching layer only determines how many of the excitons that were created by the accumulated charges will recombine radiatively. The transient signal is composed of two components (cf. Fig. 5): (1) the decay of regularly created excitons and (2) an additional signal of stored charge carriers. The regular signal consists of a monoexponential part coming from the excitons, which decay from the triplet level of $Ir(MDQ)_2(acac)$ to the ground state, and a less intensive slower component, which is visible as a deviation from the monoexponential part at later times (cf. the dashed transients in Fig. 9, where no charge accumulation occurs). The additional signal is created by the recombination of stored charge carriers after voltage turn-off. It first increases due to the time the charge carriers need to recombine and then decreases monoexponentially with the intrinsic decay time of the emitter.

To quantify this amount as a function of the position of the quenching layer, we separate the regular signal from

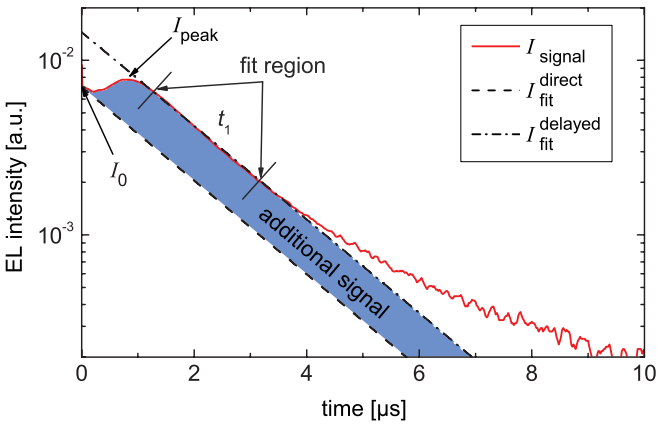


FIG. 5. (Color online) Schematic of the derivation of the area of the additional signal from the graphs of $I_{signal}$, $I_{fit}^{direct}$, and $I_{fit}^{delayed}$. Intensity of the transient peak $I_{peak}$ and intensity of the steady-state luminescence $I_0$ are shown.

the additional signal and calculate the area of the latter (cf. Fig. 5). We first fit the measured transient EL signal in its monoexponential region with a function $I_{fit}^{delayed}(t) = I_0^{delayed} e^{-t/\tau}$, where $t$ is the time after voltage turn-off and $\tau$ is the exciton lifetime. Next, we calculate the function $I_{fit}^{direct}(t) = I_0 e^{-t/\tau}$, which describes the exciton decay if no charge carriers were accumulated, with $I_0$ as the measured EL signal at $t = 0$ s. The area $A$ of the additional signal (cf. Fig. 5) can then be expressed as

$$A = \int_0^{t_1} I_{signal}(t)dt + \int_{t_1}^{\infty} I_{fit}^{delayed}(t)dt - \int_0^{\infty} I_{fit}^{direct}(t)dt, \quad (1)$$

where $t_1$ can be chosen freely along the monoexponential fitting region and $I_{signal}(t)$ is the measured transient.

Figure 4 shows the area of the additional signal $A$ as a function of the position of the quenching layer (triangles) as calculated above. Again, data points at $x = 0$ nm correspond to samples without quencher. Lowest intensity (meaning strongest quenching) occurs near the EBL interface. We therefore deduce that after voltage turn-off the recombination zone is located near the EBL, which provides direct evidence for a storage of charge carriers close to this interface. The increase of $A$ near the HBL shows that the use of the quenching layer slightly influences the recombination of accumulated charges, probably by acting as a charge trap. As the regular recombination of holes takes place at the HBL and electrons are stored closer to the anode than holes (cf. Sec. III A), we conclude that the accumulated charge carriers are electrons. This also implies that holes diffuse from the HBL side to the electrons and not vice versa, indicating that electrons are trapped and immobile.

We therefore suggest that the transient overshoot is caused by an accumulation of electrons on $Ir(MDQ)_2(acac)$ molecules as schematically illustrated in Fig. 6. Although the recombination zone is located between the EML and the HBL, electrons can be further transported on $Ir(MDQ)_2(acac)$ molecules up to the interface to the EBL. The main transport mechanism is drift caused by the applied electric field, so that holes accumulate at the HBL interface and part of the electrons

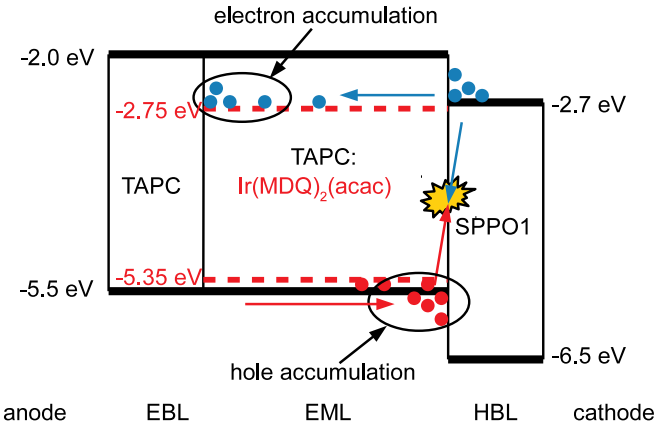


FIG. 6. (Color online) Schematic of the processes taking place in the EML during voltage application. Horizontal lines indicate the HOMO and LUMO energy levels of the materials. Holes are mainly transported on the hole transporting TAPC and accumulate at the interface to the SPPO1 HBL. Electrons partly accumulate at the interface between the HBL and the EML, where they can recombine with the accumulated holes. Because of the LUMO level matching between SPPO1 and $Ir(MDQ)_2(acac)$, electrons are also transported on the emitter molecules and accumulate at the interface to the EBL.

opposite close to the EBL, leading to charge carriers spatially separated across the EML. This is the steady-state condition during OLED operation. After turning off the electric field, the electrons and holes are able to drift and diffuse and recombine into delayed excitons, which emit additional light after voltage turn-off. Electrons are relatively immobile on the $Ir(MDQ)_2(acac)$ molecules. Hole transport after voltage turn-off is due to both diffusion and drift caused by space charges.

### C. Estimation of accumulated electron density

The amount of light originating from delayed charge carrier recombination can be directly correlated to the number of minority charge carriers in the EML after voltage turn-off. As shown later, the electron reservoir on the $Ir(MDQ)_2(acac)$ molecules is smaller than the hole reservoir on TAPC molecules. Therefore, the area $A$ of the additional signal (cf. Sec. III B) is a measure for the amount of accumulated electrons $n$, i.e., $n \propto A$. Here, we assume 100% recombination efficiency of accumulated electrons with holes after voltage turn-off. This might be a small overestimation, but it is still reasonable since after voltage turn-off holes are drifting, attracted by the electric force of the electrons. To obtain an absolute density $n$, the transient EL signal has to be calibrated to the absolute photon flux $\Phi$. We calculate $\Phi$ under Lambertian assumption by integration over the measured spectral radiant intensity $I_e$:

$$\Phi = 5\frac{\pi}{hc}\int \lambda I_e(\lambda) d\lambda. \tag{2}$$

Here, $\lambda$ denotes the wavelength, $h$ Planck's constant, and $c$ the light velocity. The factor 5 takes into account that only around 20% of the light is coupled out.[34] We now calibrate the measured time-resolved EL intensity $I_0$ during steady state (before voltage turn-off; cf. Fig. 5) with $\Phi$. The density of stored charge carriers $n$ is then described by

$$n = A\frac{\Phi}{I_0}\frac{1}{dq} \tag{3}$$

with $A$ as calculated above and $d$ as EML thickness. The radiative quantum efficiency $q$ of $Ir(MDQ)_2(acac)$ is assumed with 0.7.[35] With a photon flux of $\Phi(1\ \text{mA}) = 4.3 \times 10^{16}\ \text{s}^{-1}\text{cm}^{-2}$ at 1 mA and $\Phi(5\ \text{mA}) = 1.7 \times 10^{17}\ \text{s}^{-1}\text{cm}^{-2}$ at 5 mA, we obtain $n(1\ \text{mA}) = 5.1 \times 10^{16}\ \text{cm}^{-3}$ and $n(5\ \text{mA}) = 8.6 \times 10^{16}\ \text{cm}^{-3}$. Compared to the density of $Ir(MDQ)_2(acac)$ molecules of $9.3 \times 10^{19}\ \text{cm}^{-3}$ at 10 wt.% doping concentration, on average roughly every 1000th molecule stores an electron at 5 mA. However, electron accumulation occurs only within a narrow region close to the EBL. Additionally, it is most likely that not all accumulated electrons will recombine radiatively. Therefore, the local electron density near the EBL should be higher than the number estimated above.

### D. Effect of emitter doping concentration

The fact that charges are stored on $Ir(MDQ)_2(acac)$ is supported by the dependence of the EL overshoot and, therefore, the density of stored electrons on the $Ir(MDQ)_2(acac)$ concentration. We prepared samples with doping concentrations from 1 wt.% up to 25 wt.%. Increasing the doping concentration leads to higher current densities at a specific voltage (cf. inset of Fig. 7), which indicates that current is transported via the dopant molecules. The external quantum efficiency also increases with increasing doping concentration up to a maximum of 18 wt.%. Above this, concentration quenching[36] sets in, leading to reduced external quantum efficiency (see Supplemental Material,[29] Fig. 3).

Figure 7 shows the calculated density of accumulated electrons (cf. Sec. III C) as a function of the doping concentration. Up to a concentration of 18 wt.%, a linear behavior that provides evidence for the mechanism of charge carrier storage on $Ir(MDQ)_2(acac)$ molecules is obtained. Concerning the accumulated electrons and holes causing the transient EL

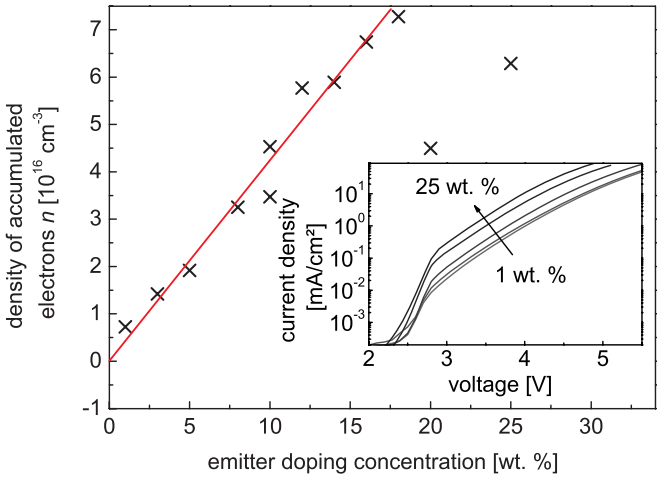


FIG. 7. (Color online) Density of accumulated electrons $n$ for different doping concentrations at an applied current of 1 mA. Up to 18 wt.%, the electron density increases linearly with doping concentration. Inset: Current density-voltage characteristics for different doping concentrations.

overshoot, it can be concluded that electrons are the minority charge carriers in the EML as the delayed signal intensity depends on the amount of stored electrons. The decrease in the density of stored electrons above 18 wt.% can have several reasons: the amount of accumulated holes might not suffice for recombination with all stored electrons. As indicated by the decrease in external quantum efficiency, concentration quenching can also play a role at high doping concentrations.[36]

Furthermore, we measured the density of accumulated charges in dependence of the applied current density and the pulse duration (cf. Secs. II and III in Supplemental Material[29]). The accumulated charge carrier density saturates at high currents and for long pulses. Interestingly, electron storage can also be observed at very short pulses indicating that electron accumulation on $Ir(MDQ)_2(acac)$ occurs prior to regular light emission.

### E. Influence of different hole-blocking layers

In this section, we investigate the mechanism of electron injection into $Ir(MDQ)_2(acac)$. Therefore, we prepared samples with different hole-blocking materials using SPPO1, bis-(2-methyl-8-chinolinolato)-(4-phenylphenolato)-aluminium(III) [$BAlq_2$, Sensient], 2,2′,2″(1,3,5-benzenetriyl)tris-(1-phenyl-1H-benzimidazole) [TPBi, Sensient], and 2,9-dimethyl-4,7-diphenyl-1,10-phenantholine [BCP, Alfa Aesar]. Figure 8 shows the corresponding current density-voltage characteristics and the external quantum efficiency. SPPO1 leads to increased voltages and reduced current densities, probably because of a poor electron mobility in SPPO1. Current density-voltage characteristics are similar for BCP and TPBi. $BAlq_2$ instead leads to current enhancement, both at low and high voltages. The SPPO1 blocker shows the lowest external quantum efficiency. Interestingly, despite the different current-voltage behavior of BCP and $BAlq_2$, both lead to an external quantum efficiency of around 15%.

Figure 9 shows the normalized EL transients of the four different samples. The highest peak intensity is obtained with the TPBi blocker, while SPPO1 and BCP cause a slight decrease. The delayed signal completely disappears using the $BAlq_2$ blocker. This behavior can be explained by considering the LUMO energy levels of the materials, which are summarized in Table I: SPPO1, TPBi, and BCP

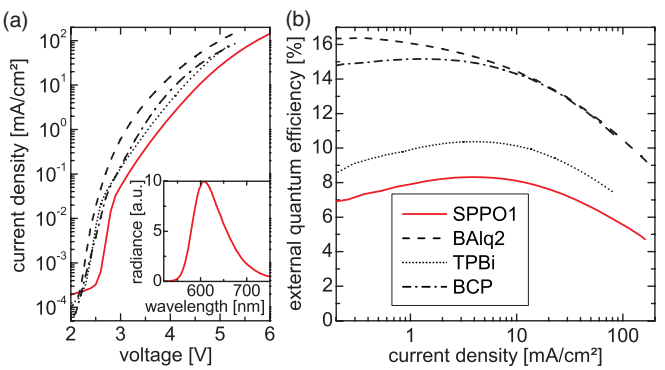


FIG. 8. (Color online) (a) Current density-voltage characteristics (inset: normalized radiance using SPPO1 as HBL) and (b) external quantum efficiency as a function of current density for different HBLs.

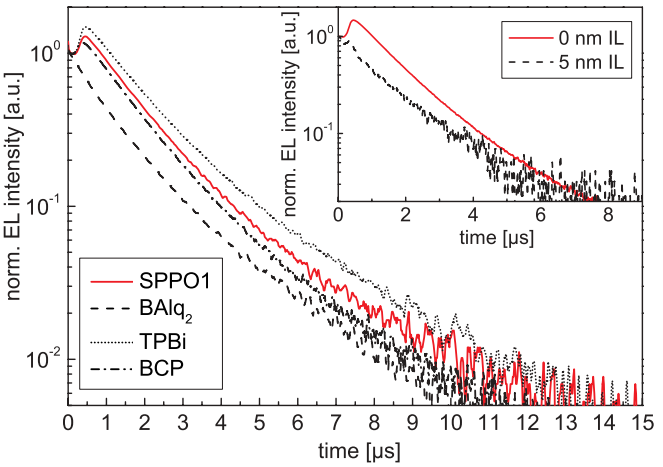


FIG. 9. (Color online) Normalized transient EL signal for samples with different HBL. A transient overshoot is visible in all samples, except with the $BAlq_2$ blocker. Inset: Normalized EL transient of a sample with 5 nm TAPC interlayer inserted between EML and HBL. The EL overshoot vanishes in this sample.

all provide similar LUMO levels of −2.7 to −2.8 eV. The LUMO level of $Ir(MDQ)_2(acac)$ is −2.75 eV. A direct injection from those blocker materials into $Ir(MDQ)_2(acac)$ is therefore energetically favorable. $BAlq_2$ instead has a LUMO level of −3.2 eV. Considering the large injection barrier of 0.5 eV at the $BAlq_2$/EML interface, electrons are not efficiently injected into $Ir(MDQ)_2(acac)$, which explains the absence of delayed recombination. In contrast to the other blocking materials, the electron transfer from the LUMO level of the BPhen:Cs-ETL (−3.0 eV[37]) to the $BAlq_2$-HBL is exotherm, which allows for low operating voltages and high EQE. Exciton formation at the EML/HBL interface is assisted by hole accumulation, thus mitigating the potentially adverse effect of the high barrier between the LUMOs of $Ir(MDQ)_2(acac)$ and $BAlq_2$.

Electron injection into $Ir(MDQ)_2(acac)$ can also be prevented by inserting a thin interlayer (IL) of pure TAPC matrix material between the HBL and the EML. The inset of Fig. 9 shows the EL transient of a device with 5 nm thick IL. The transient EL peak vanishes, which indeed shows that the electron injection is circumvented.

The fact that the EL overshoot vanishes when electrons have to cross a high energy barrier is further evidence for the injection and accumulation of electrons on $Ir(MDQ)_2(acac)$.

We also note that exchanging the matrix material TAPC with other hole-transporting matrix materials did not result in any significant change of the electron storage process (cf. Sec. IV in Supplemental Material[29]).

TABLE I. LUMO energy levels of the used HTL materials.

| Material | LUMO energy (eV) |
|---|---|
| SPPO1 | −2.7[21] |
| $BAlq_2$ | −3.2[22] |
| TPBi | −2.7[38] |
| BCP | −2.8[39] |

### F. Impedance spectroscopy

Charge carrier storage is also observed using impedance spectroscopy. The capacitance $C$ is sensitive to the charges accumulated in the device. This includes both free bulk charges and charges accumulated at the contacts to support the material polarization.[40] The capacitance of the device is calculated from the measured device impedance $Z$, assuming a parallel RC equivalent circuit:[41]

$$C(f) = \frac{-\mathrm{Im}(Z)}{2\pi f |Z|^2}, \tag{4}$$

with $f$ the applied frequency.

We measured impedance for devices with SPPO1 and $BAlq_2$ as HBL in order to show that electron storage takes place in the device containing SPPO1 but not with $BAlq_2$. Figure 10(a) shows a plot of capacitance vs voltage for a fixed frequency of 60 Hz, where two distinct features appear. First, the capacitance increases between 0.5 and 2 V only in the $BAlq_2$ device. This correlates with a charge accumulation in the HBL, as will be clarified by the capacitance spectra below. A second peak is visible around 2.5 V, representing the accumulation of electrons in the EML. For higher voltages, holes are injected into the EML and the capacitance decreases due to the recombination of free charges.[42]

The analysis of the capacitance spectra in Fig. 10(b) is crucial to correctly interpreting the capacitance-voltage plot. For 0 V dc bias, both spectra show a plateau that coincides with the geometrical capacitance of the intrinsic layers [TAPC/TAPC:Ir(MDQ)$_2$(acac)/HBL, total thickness of 40 nm], estimated to be 4.2 nF for $\epsilon = 3$. At positive bias, where a peak is visible in the capacitance-voltage plot, the two capacitance spectra differ significantly. In the case of $BAlq_2$ as HBL, the additional capacitance starts to contribute for frequencies below 10 kHz, while for SPPO1 the contribution is more pronounced but only begins below 1 kHz. This is due to the different nature and position of the charges in the device. In the $BAlq_2$ device, electrons first accumulate in the HBL due to the low LUMO level of $BAlq_2$ increasing the resistivity of the layer and inducing the flat band condition.[41] The geometrical capacitance changes from 4.2 nF to the value of 5.6 nF, given by the TAPC/TAPC:Ir(MDQ)$_2$(acac) layers (total thickness of 30 nm). This explains the increasing capacitance between 0.5 and 2.0 V for the $BAlq_2$ case.

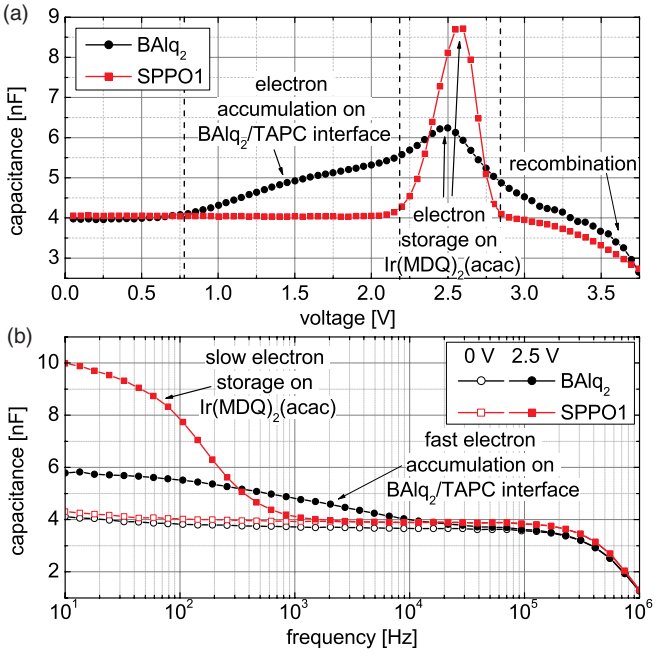


FIG. 10. (Color online) (a) Capacitance-voltage characteristics of the devices with two different HBLs, measured at 60 Hz. In the case of $BAlq_2$, the electrons accumulate in the HBL between 0.5 and 2 V. The accumulation of charges in the EML is present above 2 V and is much stronger in case of SPPO1. (b) Capacitance-frequency plot of the devices at 0 and 2.5 V. In the EML stored electrons respond much slower than electrons, which accumulate at the $BAlq_2$/EML interface.

From the capacitance-voltage measurements, a second peak at 2.5 V is visible for both devices albeit much more pronounced in the SPPO1 case. This peak is associated with the capacitive contribution at lower frequencies that reaches a plateau below 100 Hz and results from the accumulated electrons in the EML. In summary, the observations made by the time-resolved measurements could be confirmed and the slow response time indicates that electrons are indeed trapped on the Ir(MDQ)$_2$(acac) molecules as already supposed in Sec. III B.[43,44]

## IV. DELAYED RECOMBINATION IN WHITE-EMITTING PHOSPHORESCENT OLEDs

Charge carrier storage on emitter molecules is not limited to the monochromatic system discussed so far. We also observed a transient overshoot in white OLEDs with similar structure (see Ref. 7 for details on device structure). Here, the OLED consists of a multilayer stack containing Ir(MDQ)$_2$(acac), iridium(III) bis(4′,6′-difluorophenylpyridinato)tetrakis(1-pyrazolyl)borate [FIr6, Lumtec] and fac-tris(2-phenylpyridine) iridium [Ir(ppy)$_3$, Sensient] as emitting molecules and 4,4′,4″-tris (N-carbazolyl)-triphenylamine [TCTA, Sensient] and SPPO1 as matrix materials. The complete layer stack as well as the emitted spectrum and the measured transient are shown in Figs. 11 and 12, respectively. Most of the emission originates from the green emitter Ir(ppy)$_3$ while blue and red contributions are relatively small. In transient EL measurements, a clear overshoot is visible after voltage turn-off.

To investigate the responsible mechanisms for this white-emitting OLED, we performed streak camera measurements. Figures 13(a) and 13(b) show the obtained intensity, resolved both in time and wavelength. Figure 13(a) shows the entire applied pulse, while Fig. 13(b) uses a smaller time scale to magnify the region around voltage turn-off. Spectral and temporal profiles across the areas of the dashed rectangles are plotted in Figs. 13(c) and 13(d). The streak camera image shows that after voltage turn-off the maximum intensity occurs in the red region of the spectrum. During the voltage pulse, the emitted spectrum shows similar intensity for the green and the red peaks, but after turn-off, the red emission peak reaches three times the intensity of the green emission peak [cf. Fig. 13(c)]. Regarding the transient behavior in Fig. 13(d), resolved at different spectral regions, an overshoot is obtained

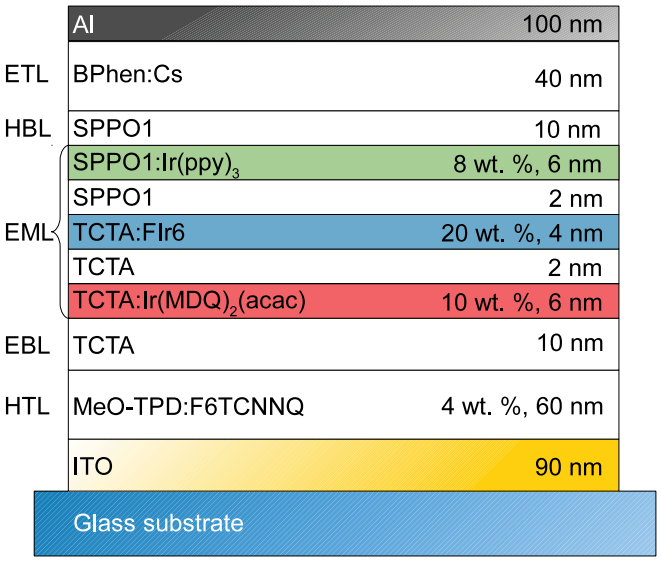


FIG. 11. (Color online) Layer stack of the white OLED device.

only from the red emission region. The transient taken in the green spectral region also shows a delayed emission, but with much lower intensity compared to the transient from the red region. Differences are also present in the decay time. Both curves show a monoexponential decay over the first 5 $\mu$s, but decay times differ between 1.8 $\mu$s (red) and 1.0 $\mu$s (green), which result from different intrinsic emitter lifetimes.[6,7]

As for the monochrome devices, electron storage on the red-emitting molecules is most likely responsible for the transient overshoot in the white device. Charge carrier storage is not observed on the blue emitter and only to a very small amount on the green emitter. This has several causes: The blue emitter is located very close to the recombination zone of regular charge carriers. Even if electrons or holes would accumulate on the emitter, they would instantly recombine due to their close distance. Therefore, delayed recombination can not be observed. Electron trapping on the green emitter is possible as the LUMO level of $Ir(ppy)_3$ is lower than that of SPPO1. However, delayed recombination is hardly observed in the measured transients because the 2 nm interlayer of SPPO1 hinders hole injection (both before and after voltage turn-off). Instead, the emission from $Ir(ppy)_3$ is mostly fed by free excitons diffusing to the emitter molecules.

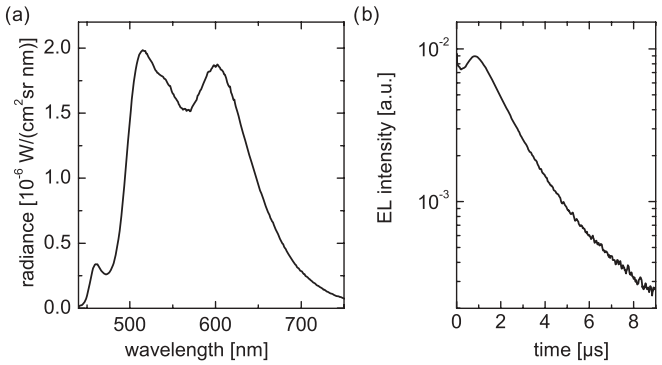


FIG. 12. (a) Spectral radiance and (b) transient EL intensity of the white OLED.

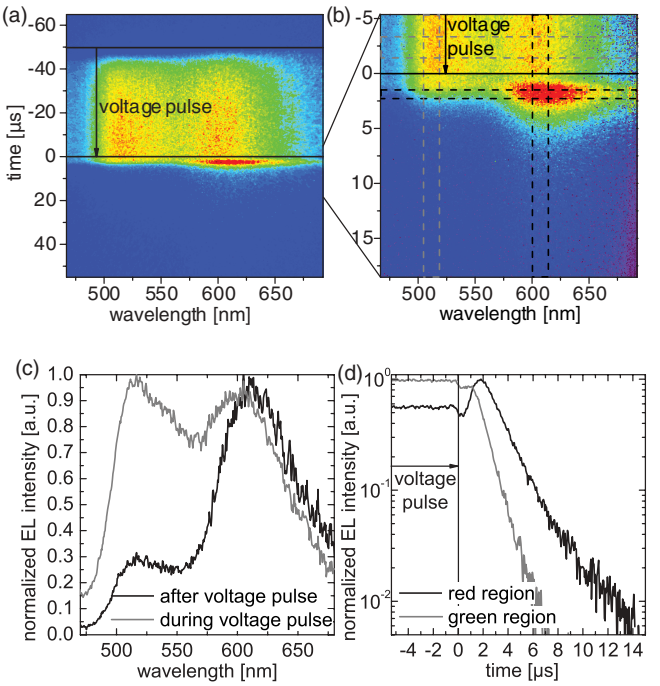


FIG. 13. (Color online) (a) and (b) Streak camera images of the white OLED. The very high intensity around 610 nm shows that the delayed recombination originates from the red emitter molecules. (c) and (d) Profiles, as obtained by integration over the dashed rectangles in part (b). After voltage turn-off most of the emission originates from the red emitter.

Interestingly, we observe a transient overshoot of the blue emission in samples containing a double EML with TAPC:FIr6/SPPO1:FIr6 (cf. Supplemental Material,[29] Fig. 4). We suggest that in this case holes are also transported via the FIr6 emitter and can accumulate at the interface to the HBL. Nevertheless, the dominant process in the presented white OLED is charge carrier storage on $Ir(MDQ)_2(acac)$, as the overshoot emission mainly originates from the red emitter. Energy transfer from FIr6 to $Ir(MDQ)_2(acac)$ is excluded because of the energy barrier of the 2 nm thick TCTA interlayer.[7]

## V. SUMMARY AND CONCLUSION

In summary, we investigated the time-dependent behavior of an OLED stack containing the red-emitting phosphor $Ir(MDQ)_2(acac)$. We observed a transient overshoot after voltage turn-off, which we attribute to charge carrier storage on the red emitter while applying an electric field. The prerequisites for this process are the resonant LUMO levels of the dopant and the hole-blocking material, which allow for efficient electron injection into the red emitter molecules.

Measuring the profile of the emission zone enabled us to directly localize where the electron storage takes place inside the EML, namely, near the interface to the electron blocking layer. Electron accumulation and storage depends on the applied electric field, and the transient overshoot can be suppressed by application of a positive field after voltage turn-off. We found a direct proportionality between the concentration of the emitter and the number of accumulated electrons, which explains electron accumulation on $Ir(MDQ)_2(acac)$ molecules.

Additionally, we demonstrated charge carrier storage via impedance spectroscopy showing that electrons are trapped on the $Ir(MDQ)_2(acac)$ molecules and are, therefore, immobile.

We suspect that charge carrier storage inside the EML decreases the device efficiency. First, excitons may be quenched by the additional polarons. Second, the accumulated charges create an additional electric field, which may lead to field-induced quenching. Finally, if stored electrons recombine nonradiatively with traps, the electron reservoir needs to be refilled. This would remove electrons from the regular recombination zone and thus decrease the external quantum efficiency.

The observed process of charge carrier storage is not limited to the red-emitting layer stack. Even in white OLEDs with very thin emission layers, charge carrier accumulation can occur. Therefore, we emphasize that unwanted charge carrier storage may be present in many OLED structures, where the dopant energy level of the minority charge carrier matches the energy level of the blocker. With the measurement techniques discussed here it is not only possible to identify charge carrier storage, but also to quantify the density of the accumulated charge carriers.

## ACKNOWLEDGMENTS

We thank Simone Hofmann, Axel Fischer, and Hans Kleemann for fruitful discussions. The work leading to these results has received funding from the German BMBF under Contract No. 13N11060 (R2Flex).

*caroline.weichsel@iapp.de; www.iapp.de

†Present address: Massachusetts Institute of Technology, 77 Massachusetts Avenue, Cambridge, MA 02139, USA.

[1] S. Reineke, K. Walzer, and K. Leo, Phys. Rev. B **75**, 125328 (2007).

[2] J. Kalinowski, W. Stampor, J. Mezyk, M. Cocchi, D. Virgili, V. Fattori, and P. Di Marco, Phys. Rev. B **66**, 235321 (2002).

[3] T. C. Wong, J. Kovac, C. S. Lee, L. S. Hung, and S. T. Lee, Chem. Phys. Lett. **334**, 61 (2001).

[4] A. Rihani, L. Hassine, J.-L. Fave, and H. Bouchriha, Org. Electron. **7**, 1 (2006).

[5] M. A. Baldo, C. Adachi, and S. R. Forrest, Phys. Rev. B **62**, 10967 (2000).

[6] S. Reineke, F. Lindner, G. Schwartz, N. Seidler, K. Walzer, B. Lüssem, and K. Leo, Nature **459**, 234 (2009).

[7] C. Weichsel, S. Reineke, M. Furno, B. Lüssem, and K. Leo, J. Appl. Phys. **111**, 033102 (2012).

[8] Y. H. Tak, J. Pommerehne, H. Vestweber, R. Sander, H. Bässler, and H. H. Hörhold, Appl. Phys. Lett. **69**, 1291 (1996).

[9] V. R. Nikitenko, V. I. Arkhipov, Y.-H. Tak, J. Pommerehne, H. Bässler, and H.-H. Hörhold, J. Appl. Phys. **81**, 7514 (1997).

[10] D. J. Pinner, R. H. Friend, and N. Tessler, J. Appl. Phys. **86**, 5116 (1999).

[11] L. Hassine, H. Bouchriha, J. Roussel, and J.-L. Fave, Appl. Phys. Lett. **78**, 1053 (2001).

[12] L. Hassine, H. Bouchriha, J. Roussel, and J.-L. Fave, J. Appl. Phys. **91**, 5170 (2002).

[13] Z. D. Popovic and H. Aziz, J. Appl. Phys. **98**, 013510 (2005).

[14] Y. Luo and H. Aziz, Adv. Funct. Mater. **20**, 1285 (2010).

[15] Y. Luo and H. Aziz, J. Appl. Phys. **107**, 094510 (2010).

[16] R. Liu, Z. Gan, R. Shinar, and J. Shinar, Phys. Rev. B **83**, 245302 (2011).

[17] S. Reineke, F. Lindner, Q. Huang, G. Schwartz, K. Walzer, and K. Leo, Phys. Status Solidi B **245**, 804 (2008).

[18] D. Song, S. Zhao, Y. Luo, and H. Aziz, Appl. Phys. Lett. **97**, 243304 (2010).

[19] M.-T. Lin, M. Li, W.-H. Chen, M. A. Omary, and N. D. Shepherd, Solid-State Electron. **56**, 196 (2010).

[20] Y. Zheng, S. H. Eom, N. Chopra, J. W. Lee, F. So, and J. G. Xue, Appl. Phys. Lett. **92**, 223301 (2008).

[21] S. O. Jeon, K. S. Yook, C. W. Joo, and J. Y. Lee, Appl. Phys. Lett. **94**, 13301 (2009).

[22] R. Meerheim, S. Scholz, S. S. Olthof, G. Schwartz, S. Reineke, K. Walzer, and K. Leo, J. Appl. Phys. **104**, 14510 (2008).

[23] The voltage actually applied to the OLED is lower than the measured one, because of voltage drops in the cables. Therefore, we measure the devices at constant current.

[24] K. Walzer, B. Maennig, M. Pfeiffer, and K. Leo, Chem. Rev. **107**, 1233 (2007).

[25] R. Meerheim, B. Lüssem, and K. Leo, Proc. IEEE **97**, 1606 (2009).

[26] N. Chopra, J. Lee, J. G. Xue, and F. So, IEEE Trans. Electron Devices **57**, 101 (2010).

[27] S. E. Jang, C. W. Joo, S. O. Jeon, K. S. Yook, and J. Y. Lee, Org. Electron. **11**, 1059 (2010).

[28] S. Reineke, T. C. Rosenow, B. Lüssem, and K. Leo, Adv. Mater. **22**, 3189 (2010).

[29] See Supplemental Material at http://link.aps.org/supplemental/10.1103/PhysRevB.86.075204 for supplemental figures and further investigations on the influence of the applied current, pulse duration, and matrix material.

[30] W. Ji, L. Zhang, R. Gao, L. Zhang, W. Xie, H. Zhang, and B. Li, Opt. Express **16**, 15489 (2008).

[31] A. Köhler and H. Bässler, Mater. Sci. Eng. R **66**, 71 (2009).

[32] L. Zhang, B. Li, B. Lei, Z. Hong, and W. Li, J. Lumin. **128**, 67 (2008).

[33] D. L. Dexter, J. Chem. Phys. **21**, 836 (1953).

[34] C. Adachi, M. A. Baldo, M. E. Thompson, and S. R. Forrest, J. Appl. Phys. **90**, 5048 (2001).

[35] T. D. Schmidt, D. S. Setz, M. Flämmich, J. Frischeisen, D. Michaelis, B. C. Krummacher, N. Danz, and W. Brütting, Appl. Phys. Lett. **99**, 163302 (2011).

[36] Y. Kawamura, J. Brooks, J. J. Brown, H. Sasabe, and C. Adachi, Phys. Rev. Lett. **96**, 017404 (2006).

[37] S. H. Eom, Y. Zheng, E. Wrzesniewski, J. Lee, N. Chopra, F. So, and J. G. Xue, Org. Electron. **10**, 686 (2009).

[38] J. H. Jou, C.-P. Wang, M. H. Wu, P.-H. Chiang, H.-L. Lin, H. C. Li, and R.-S. Liu, Org. Electron. **8**, 29 (2007).

[39] M. Cocchi, D. Virgili, C. Sabatini, and J. Kalinowski, Chem. Phys. Lett. **421**, 351 (2006).

[40] J. Jamnik and J. Maier, Phys. Chem. Chem. Phys. **3**, 1668 (2001).

[41] E. Barsoukov and J. Macdonald, *Impedance Spectroscopy: Theory, Experiment and Applications*, 2nd ed. (Wiley, New York, 2005).

[42] H. H. P. Gommans, M. Kemerink, and R. A. J. Janssen, Phys. Rev. B **72**, 235204 (2005).

[43] D. Ray, L. Burtone, K. Leo, and M. Riede, Phys. Rev. B **82**, 125204 (2010).

[44] L. Burtone, D. Ray, K. Leo, and M. Riede, J. Appl. Phys. **111**, 064503 (2012).